

**UNCLASSIFIED**

---

---

**AD 295 486**

*Reproduced  
by the*

**ARMED SERVICES TECHNICAL INFORMATION AGENCY  
ARLINGTON HALL STATION  
ARLINGTON 12, VIRGINIA**



---

---

**UNCLASSIFIED**

NOTICE: When government or other drawings, specifications or other data are used for any purpose other than in connection with a definitely related government procurement operation, the U. S. Government thereby incurs no responsibility, nor any obligation whatsoever; and the fact that the Government may have formulated, furnished, or in any way supplied the said drawings, specifications, or other data is not to be regarded by implication or otherwise as in any manner licensing the holder or any other person or corporation, or conveying any rights or permission to manufacture, use or sell any patented invention that may in any way be related thereto.

295486

295 486

GA-3616

MANAGED BY ASTIA

AD-110

TRANSIENT RADIATION EFFECTS  
ON COAXIAL CABLES

Contract DA36-039 SC-89196

SPECIAL TECHNICAL REPORT

U. S. ARMY ELECTRONICS RESEARCH  
AND DEVELOPMENT LABORATORY  
FORT MONMOUTH, NEW JERSEY

General Atomic Division of General Dynamics Corporation  
San Diego, California

December 18, 1962

ASTIA  
FEB 4 1963  
ASTIA

**TRANSIENT RADIATION EFFECTS  
ON COAXIAL CABLES**

**Contract DA36-039SC-89196  
Signal Corps Technical Guidelines for PR and C  
No. 62-ELP/D-4024, dated 13 October 1962**

---

**SPECIAL TECHNICAL REPORT**

**Object: To determine the differential  
mechanism by which a pulse  
of nuclear radiation affects  
the electrical characteristics  
of certain electronic parts.**

**Authors: G. R. Hopkins, A. L. A. Weiman  
and D. E. Willis**

**December 18, 1962**

## ABSTRACT

An investigation into the radiation effects of gamma and neutron radiation on polyethylene coaxial cable has been started. By a series of tests made in the General Atomic TRIGA Mark F reactor, individual effects due to gamma, fast, and thermal neutron flux have been separated and analyzed. Gamma radiation produces a current nearly proportional to incident flux with the central wire at a negative potential. Thermal neutron flux also produces a nearly proportional signal but with the central wire going positive. Fast neutron flux produces a positive-going signal having two components. One component is proportional to flux; the other produces a very large initial signal but saturates quickly. Saturation occurs as integrated fast neutron flux increases and is not time dependent. Varying amounts and types of shielding provided large changes in relative components of flux, both with pulsing and steady-state modes of operation. The data were analyzed for each type of radiation.

Although the effects have been analyzed in some detail, more investigation is required to supply more accurate numbers. Special experiments should provide clues as to which of several possible mechanisms are involved.

## CONTENTS

	<u>Page</u>
ABSTRACT	ii
LIST OF FIGURES	iv
I INTRODUCTION	1
II EXPERIMENTAL ARRANGEMENT	3
2.1 REACTOR FACILITY	3
2.2 MEASUREMENT CIRCUITS	7
2.3 SPECIAL CABLE	7
III FLUX MEASUREMENTS	13
IV DATA AND DISCUSSIONS	17
4.1 GAMMA DATA	17
4.2 THERMAL NEUTRON DATA	22
4.3 FAST NEUTRON DATA	24
4.4 ANALYSIS OF DATA	30
4.4.1 <u>Gamma Ray Effects</u>	30
4.4.2 <u>Thermal Neutron Effects</u>	32
4.4.3 <u>Fast Neutron Effects</u>	35
V CONCLUSIONS	41
VI ACKNOWLEDGEMENTS	43
REFERENCE	43

## FIGURES

	<u>Page</u>
1. Typical TRIGA Mark F reactor \$2.91 pulse shape	4
2. Position of void tank and graphite tank relative to reactor core	5
3. Block diagram of pulse measurement circuit	8
4. Block diagram of pulse timing circuit	9
5. Block diagram of integrating circuit	10
6. Copper coaxial cable	11
7. Relative timing between RG-58, BF <sub>3</sub> , and reactor power signals	14
8. Relative timing between carbon ion chamber and reactor power signals	15
9. Signals from cadmium-covered RG-58 in graphite and in core	18
10. Signals from bare and cadmium-covered copper coaxial cable	19
11. Signal from RG-58 irradiated at LINAC	20
12. Integrated signal from cadmium-covered RG-58 in graphite	21
13. Signals from bare RG-58 in graphite	23
14. Integrated signal from bare RG-58 in graphite	25
15. Signals from bare RG-58 in void tank	26
16. Sequence of signals from bare RG-58 in void tank	27
17. Integration of signal in Fig. 15A	28
18. Integrated signal from bare RG-58 in void tank	29
19. Prompt component of fast neutron signal in RG-58	36

## I: INTRODUCTION

The transient electrical signals from a length of coaxial cable inserted in several positions in the TRIGA Mark F reactor were measured during reactor pulses. Cadmium shielding and various irradiation facilities have been used to obtain a spectral separation of the neutron fluxes as well as variations in the gamma dose levels. The effects of thermal neutrons, fast neutrons, and gamma rays have been observed individually in both pulsing and steady-state operation. An unusual and heretofore unobserved effect was determined to be a result of neutron irradiation. The purpose of this report is to describe the measurements and provide preliminary analyses in explanation of the electrical response of the cable due to neutron irradiations. These results may also describe some of the results observed in cables irradiated with GODIVA-type reactors.

## II: EXPERIMENTAL ARRANGEMENT

### 2.1 REACTOR FACILITY

The irradiations of coaxial cables reported in this paper were conducted at three locations in the reactor facility; in-core, a graphite tank, and a void tank.

In all the transient (or pulsing) operations reported here, the TRIGA Mark F reactor was pulsed by the step insertion of \$2.91 of excess reactivity above delayed critical. The monitor signals shown on the lower oscillogram traces in the various illustrations are proportional to reactor power yields. Figure 1 shows the shape of a typical pulse; the peak power level during the pulse is about 1600 Mw-(thermal) while the total integrated power (prompt pulse) is about 20 Mw -secs.

The in-core experiments were made by lowering an aluminum tube into fuel element position No. G-18 in the outer ring of the reactor core. Figure 2A shows the position of position G-18 relative to the other irradiation facilities.

Figure 2A also shows the void tank in position against the core. The void tank was modified to obtain a high fast neutron flux, low gamma flux, and essentially no thermal neutron flux. This was obtained by placing a 1/4 in. boral sheet and 4 in. of lead between No. 2 hole in the void tank and the core, and 1/2 in. of lead behind the No. 2 hole to reduce back scattering. A 1/4 in. sheet of borated plastic was wrapped around the second hole to further reduce the thermal neutron flux.

The graphite tank, as shown in Fig. 2B, is located next to the core in a manner similar to the void tank. For the coaxial cable irradiations, the graphite tank No. 2 tube was used and approximately 31 in. of graphite was placed between the tube and core. In this position the cable was essentially exposed only to thermal neutrons except for a very small gamma flux. By covering the cable with a sheet of cadmium, the thermal neutron flux could be reduced to an insignificant value compared to the gamma flux. The graphite tank was therefore used to observe the effects on the cable from both thermal neutron and gamma radiation.

The relative fluxes in the three positions are discussed in Section III and summarized in Table 1.

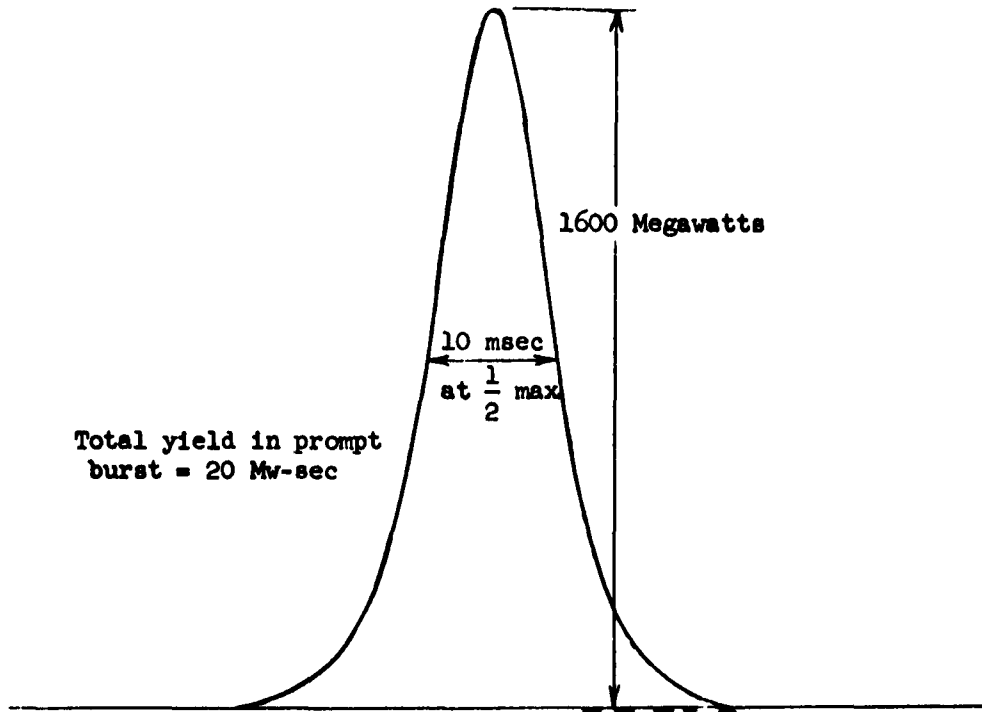


Fig. 1-- Typical TRIGA Mark F reactor \$2.91 pulse shape

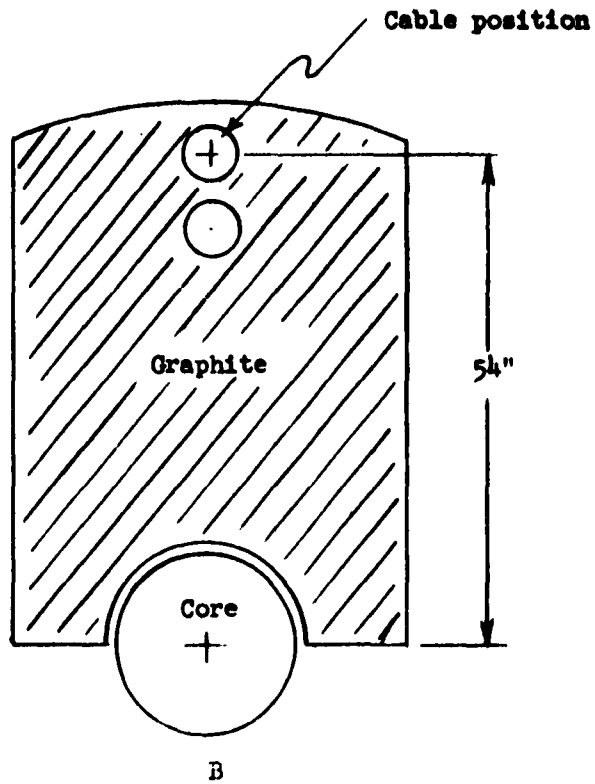
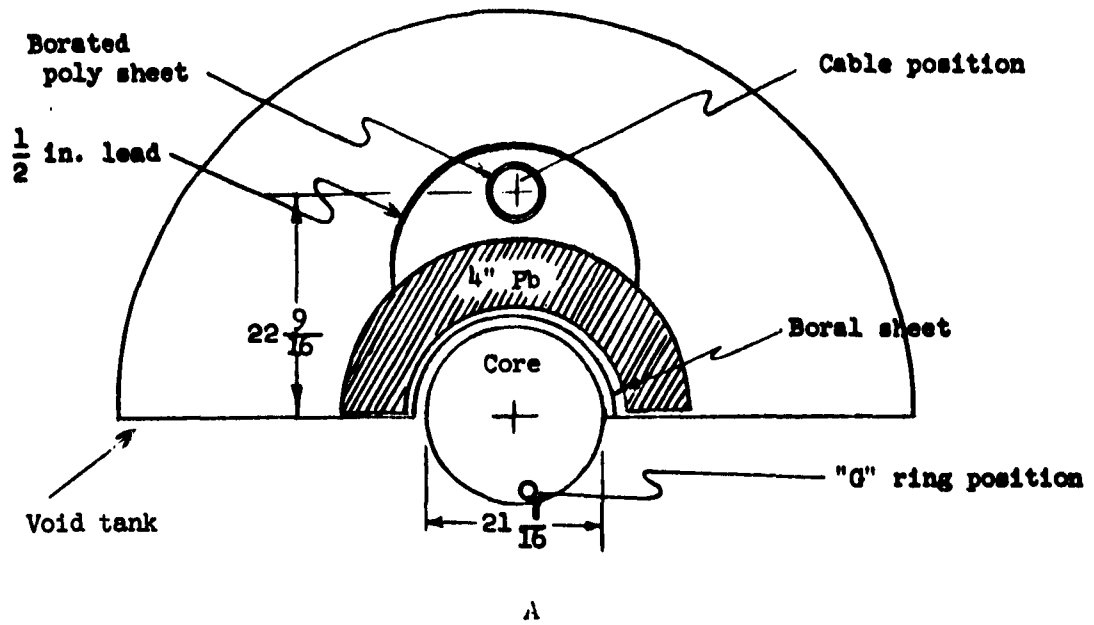


Fig. 2--Position of void tank and graphite tank relative to reactor core

Table 1

FLUXES AT IRRADIATION POSITIONS

	Thermal Column	Thermal Column (Cd Covered)	In-Core (G-Ring)	In-Core (G-Ring Cd Covered)	Void Tank (Lead and Boron Shields)
Gamma Dose (Rads/pulse)	110	940	$3.5 \times 10^5$	$4.2 \times 10^5$	780
Gamma Dose Rate (Rads/Mw-sec)	5.5	47	$1.8 \times 10^4$	$2.1 \times 10^4$	39
Peak Gamma Dose Rate* (Rads/sec)	$8.7 \times 10^3$	$7.4 \times 10^4$	$2.7 \times 10^7$	$3.3 \times 10^7$	$3.5 \times 10^4$
Peak Thermal Neutron Flux* (nv)	$9.4 \times 10^{13}$	0	$2.0 \times 10^{16}$	0	$9.3 \times 10^{12}$
Epicadmium Flux (Relative)	4.2	4.2	$4.5 \times 10^4$	$4.85 \times 10^4$	$3.1 \times 10^2$
Cadmium Ratio	223	—	10.8	—	1.3
Sulfur flux † (> 3.0 Mev)	—	—	—	—	$3 \times 10^{11}$
Plutonium Flux † (> 10 kev)	—	—	—	—	$5 \times 10^{12}$

\*Maximum at peak reactor power during pulse (1600 Mw)

† nvt/20 Mw-sec

In each of the three positions the end of the cable to be irradiated was doubled back on itself to form a loop in order to keep the termination of the cable out of the radiation field, thereby reducing end effects. When lowered into position, the cut end of the cable was approximately 4 feet above the center line of the core.

## 2.2 MEASUREMENT CIRCUITS

Figure 3 is a block diagram of the circuit used for pulse measurements on the cables. Since most of the measurements were made with zero voltage on the cable, the power supply was not connected. The 100 k $\Omega$  resistor was selected to obtain sufficient signal to observe on the scope. The signal from the cable was always displayed on the upper trace of a dual trace oscilloscope. The output of the Keithley microammeter, which is proportional to reactor power, was displayed on the lower trace of the scope.

To observe the relative timing between peak flux in the core and peak flux in either of the two tank positions, the circuit in Fig. 4 was used. This permitted the cable signal and the peak fluxes to be simultaneously displayed on the oscilloscope.

During steady-state irradiation of the cables, it was necessary to observe the integrated effect. Figure 5 is a simplified block diagram of the integrating system used for this purpose.

## 2.3 SPECIAL CABLE

Figure 6 shows the copper coaxial cable used to observe the effect of removing the dielectric from a coaxial cable. The copper coaxial cable was irradiated in the graphite tank with and without cadmium covering. When lowered into the tank the tube was long enough to keep the junction of the copper coaxial cable to the RG-58 cable well out of the radiation field.

Prior to irradiation the tube was evacuated to approximately 100  $\mu$  Hg and the valve closed. The vacuum pump was disconnected during the irradiation. Results of the irradiation are discussed in Section IV.

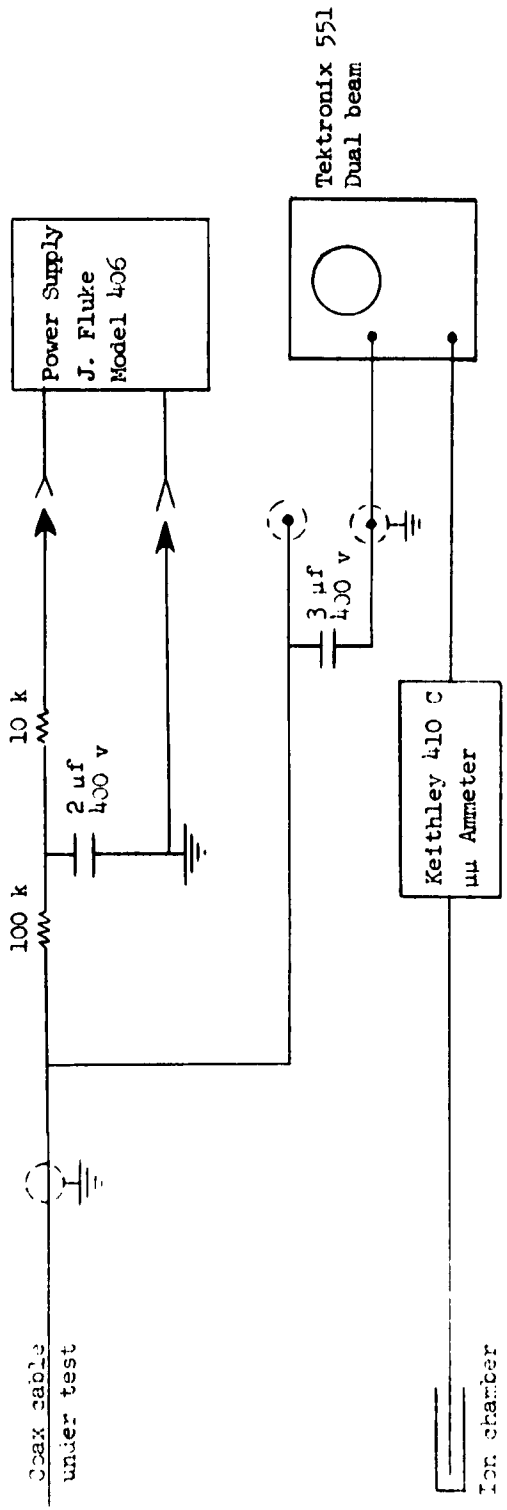


Fig. 3--Block diagram of pulse measurement circuit

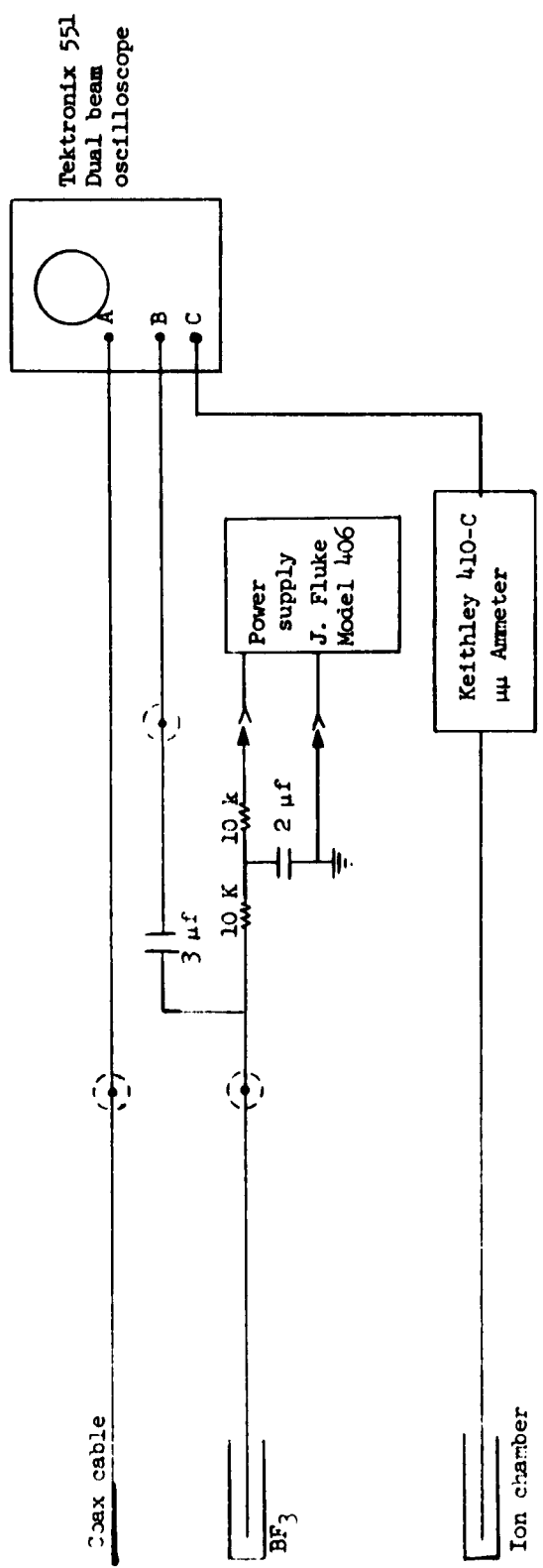


Fig. 4--Block diagram of pulse timing circuit

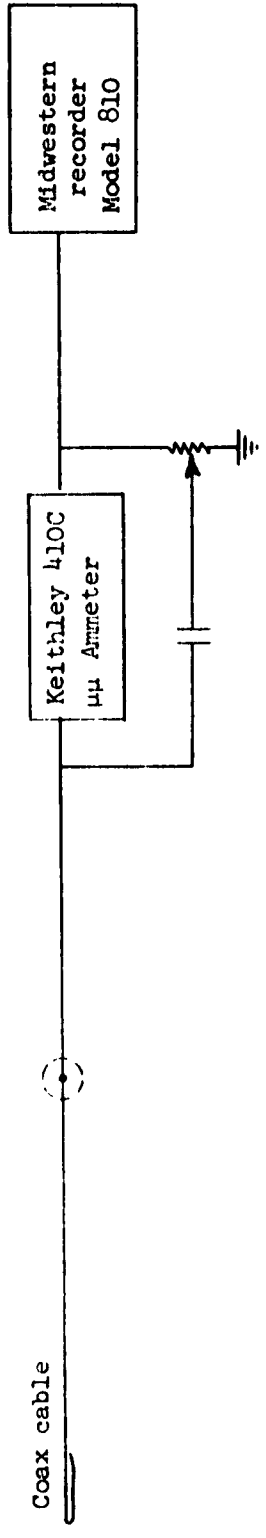


Fig. 5 -- Block diagram of integrating circuit

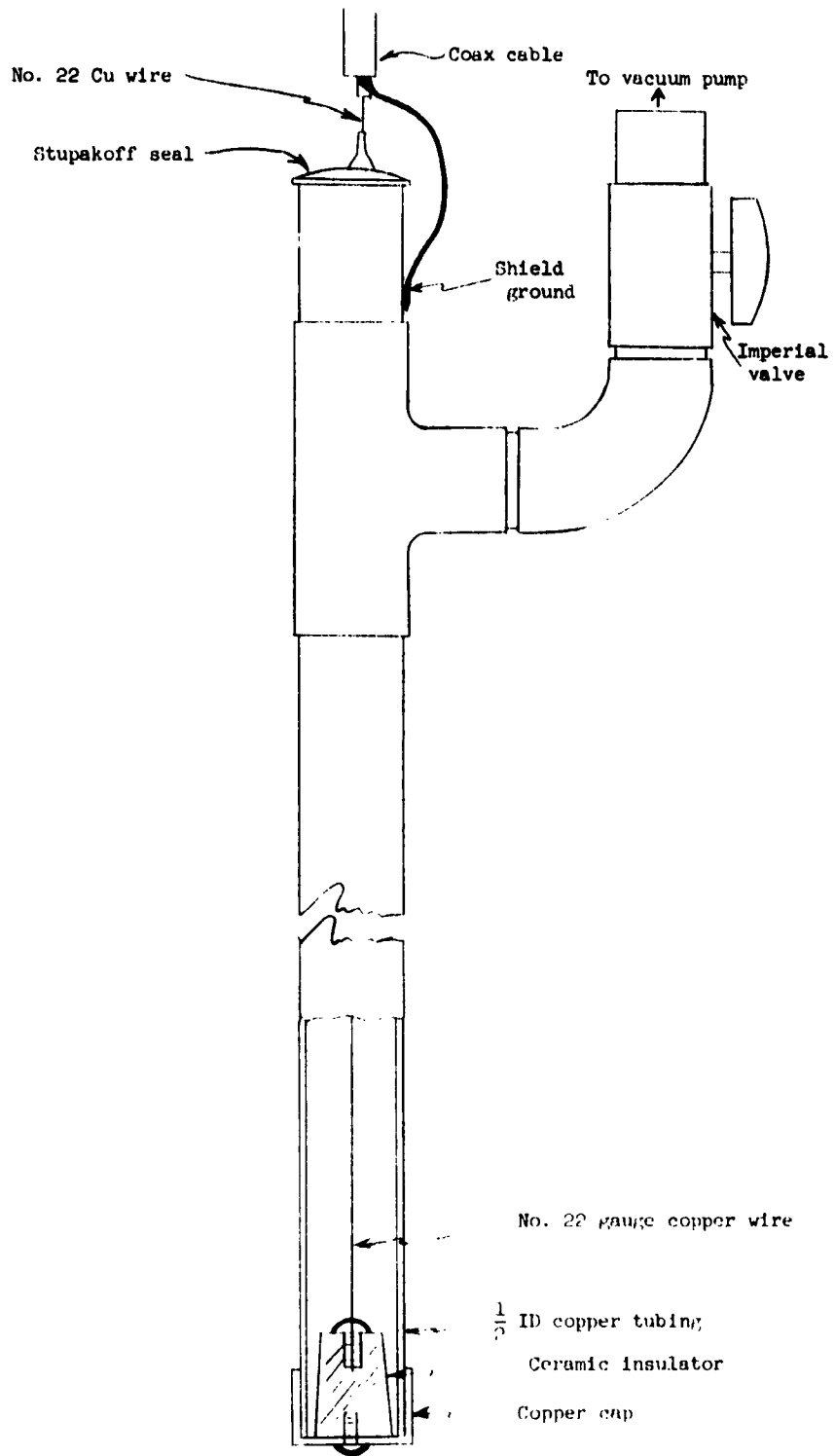


Fig. 6--Copper coaxial cable

### III. FLUX MEASUREMENTS

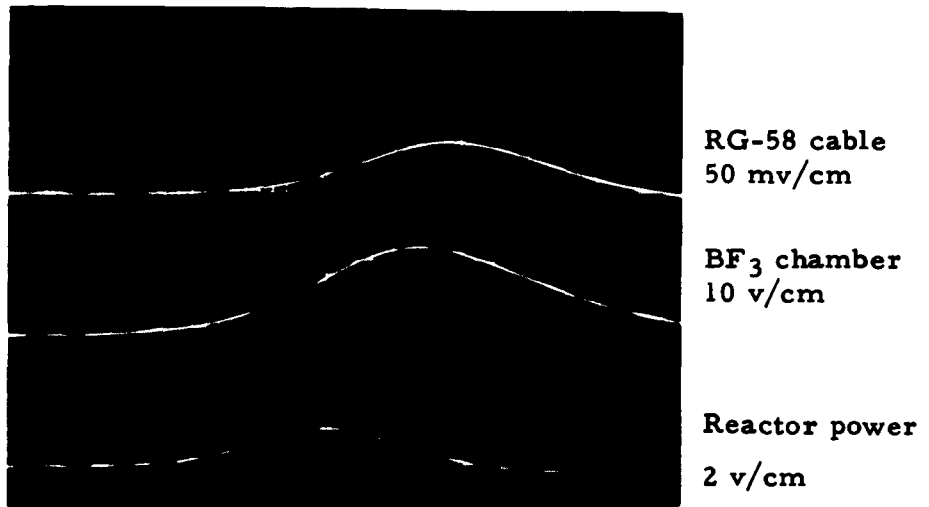
Measurements of the fast neutron, thermal neutron, and gamma fluxes were made in all of the irradiation positions. Gold foil activation, both with and without a cadmium cover, was used for the thermal flux measurements. The epicadmium activation also gave relative measurements of the fast flux, although such data are difficult to interpret on an absolute scale. The fast flux data from the gold activation is primarily a measure of the very low end of the spectrum, i. e., from 0.45 ev up. Sulfur activation was also used for fast neutron measurements in the fast neutron facility. The neutron energy threshold for activation is 2.5 to 3 Mev; thus this gives a measure of the very high end of the neutron spectrum. Preliminary measurements with fission foils were made for the neutron spectrum between these two extremes. These data are necessary since the spectra vary considerably between the several positions because of the different geometries and materials around the irradiation facilities.

Gamma dosimetry was performed primarily with chemical dosimeters of a standard commercial type. These were exposed with both lithium shields and cadmium shields since the dosimeters are also sensitive to thermal neutrons. The cadmium shield was used to duplicate the cadmium-covered cable geometry since cadmium produces a considerable dose from the neutron capture gammas. The lithium shield data gives the gamma dose equivalent to the bare cable irradiation. In addition, a small carbon ion chamber was used to obtain data on the gamma flux as a function of time. The activation foils and the chemical dosimeters give only the integral dose. The time dependence of the flux is of importance in interpretation, particularly in the graphite column. In this facility, the thermal neutron pulse is delayed by 4-6 msec from the reactor pulse. A  $\text{BF}_3$  filled ion chamber inserted in the graphite column position and connected to the oscillograph was used to determine the timing relative to the monitor signal. Figure 7 (Tr. 3585) shows the reactor pulse and the neutron pulse in the graphite column together with a typical cable signal to show the time separation.

The carbon ion chamber was used in the graphite tank to indicate relative timing of the peak of the gamma flux seen by the cable at that position (See Fig. 8, Tr. 3691). The peak thermal flux, the gamma flux, and the gamma flux produced in cadmium, all follow the monitor signal by 4-6 milliseconds.

---

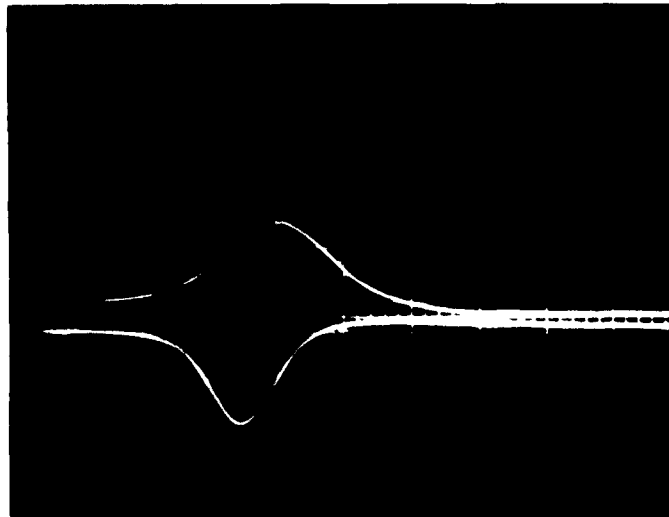
\*The chemical dosimeters, sulfur pellets, and readout were purchased from Edgerton, Germeshausen and Grier Corp., Santa Barbara, California.



Sweep - 4 msec/cm

Fig. 7 -- Relative timing between RG-58,  
BF<sub>3</sub>, and reactor power signals

400 v on Ion chamber



Ion chamber  
5 v/cm; +6 v

Reactor power  
2 v/cm; 2.8 v

Sweep - 10 msec/cm  
Approx. time delay - 5 msec

Fig. 8 -- Relative timing between carbon ion chamber and reactor power signals

The estimates now available on the fluxes at the various positions in the core are shown in Table 1. More accurate values will be obtained in the near future.

## IV. DATA AND DISCUSSIONS

### 4.1 GAMMA DATA

In order to irradiate cables with a predominately gamma flux, the graphite tank was used, with a wrapping of 0.020 in. cadmium sheet around the sample. Measurements indicate flux on the order of 940 rads/pulse or 47 rads/Mw-sec. Neutron fluxes in this facility were checked and found to contribute little to the cable signal. Figures 9A and 9C (Tr. 3682 and 3686) are typical cable signals from a pulse. In all cases checked, the signal due to gamma fluxes is negative and nearly proportional to the intensity. There is no large saturation effect and no change in sensitivity due to previous neutron exposure. Figures 9A, 9B, and 9C (Tr. 3682, 3685 and 3686) show that there is no signal change in gamma fields when the cable receives a large irradiation in the core between runs in cadmium-covered graphite. The apparent time delay between the power and the cable signals follows the actual gamma flux in the facility, as shown in Fig. 8 (Tr. 3691), where a carbon chamber is substituted for the cable.

The copper cable, which substitutes a partial vacuum for the polyethylene dielectric of a normal cable, produces a similar signal in the graphite position; the peak value when the cable is cadmium covered about twice that of the bare copper cable (See Fig. 10, Tr. 3579 and 3580).

Previous measurements made on the General Atomic Linear Accelerator (LINAC), with zero volts on the cable which was irradiated with a 4.5  $\mu$ sec, 30 Mev electron beam, produced negative signals approximately proportional to the flux, with no unusual initial effects evident (See Fig. 11).

Since all evidence indicates that a secondary emission signal due to gamma flux is negative and nearly proportional, runs were made at 1 Mw steady-state on cadmium-covered RG-58, with the cable connected to the integrator. Figure 12 shows a linear relationship with a slope of  $2.4 \times 10^{-10}$  coulombs/Mw-sec for this length of cable. The cable signal due to gamma flux for this series of experiments then may be taken as

$$\frac{2.4 \times 10^{-10} \text{ coulombs/Mw-sec}}{47 \text{ Rads/Mw-sec}} = 5.1 \times 10^{-12} \frac{\text{coulombs}}{\text{rad}}$$

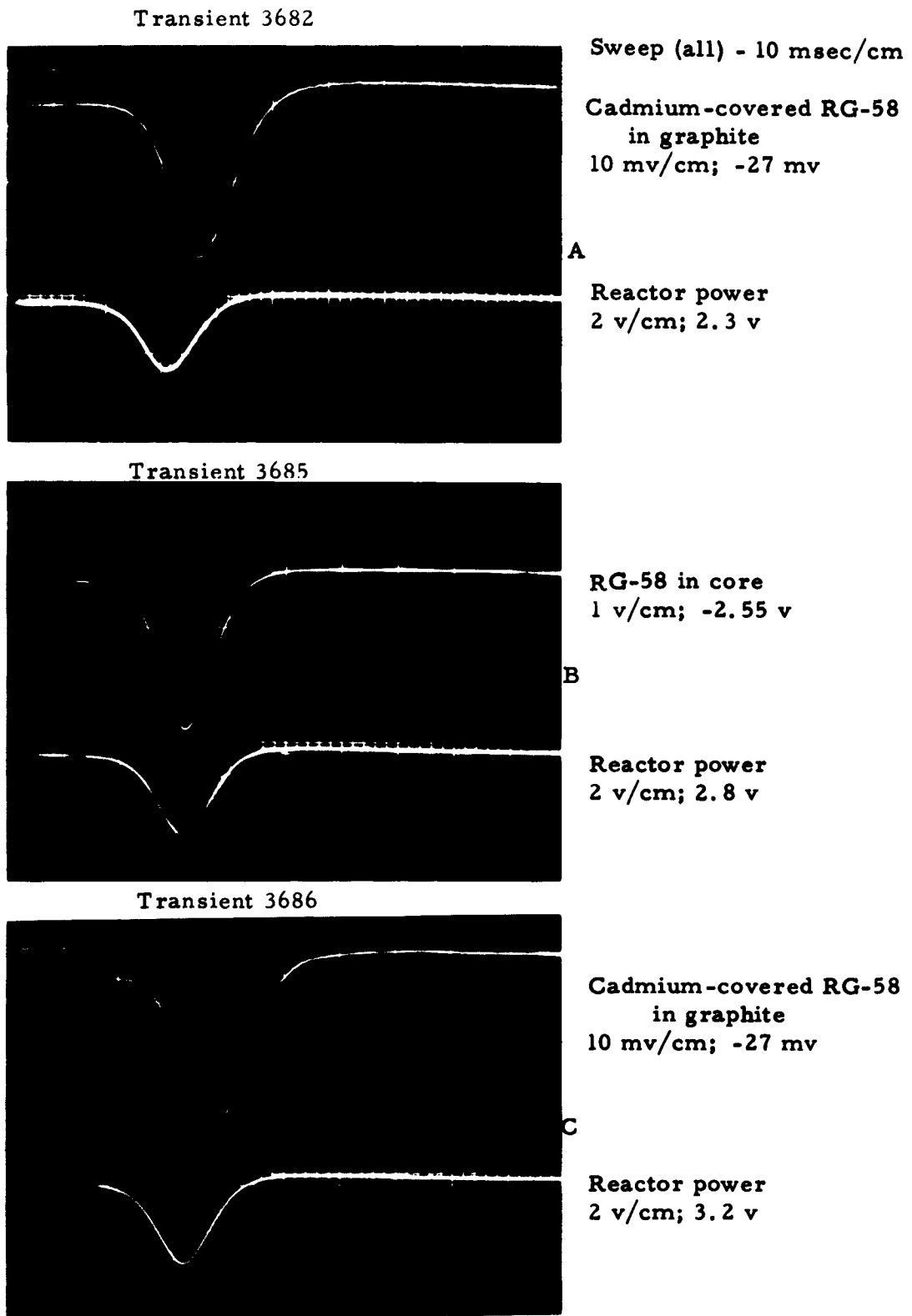
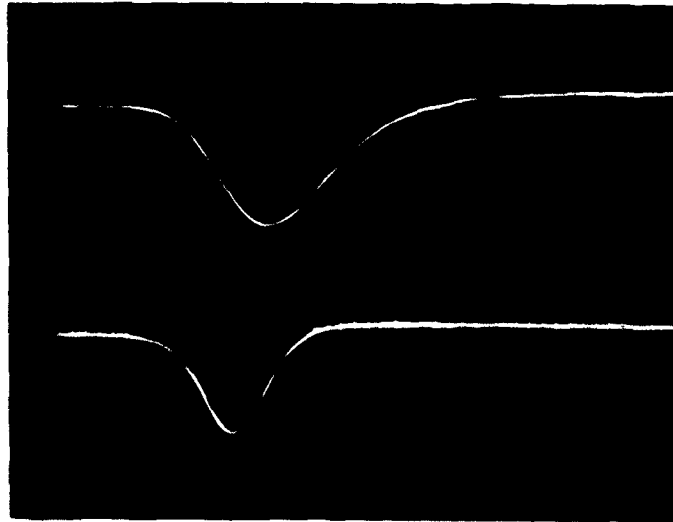


Fig. 9 -- Signals from cadmium-covered RG-58 in graphite and in core

Transient 3579



Cadmium-covered  
Cu coaxial cable in  
graphite  
20 mv/cm; +0.032 v  
delayed

Reactor power  
2 v/cm; 2.9 v

Sweep 10 msec/cm (all)

Transient 3580



Bare Cu coaxial  
cable in graphite  
10 mv/cm; -0.015 v  
delayed

Reactor power  
2 v/cm; 2.9 v

Fig. 10 -- Signals from bare and cadmium-covered copper coaxial cable



Cable signal

LINAC pulse

Fig. 11 -- Signal from RG-58  
irradiated at LINAC

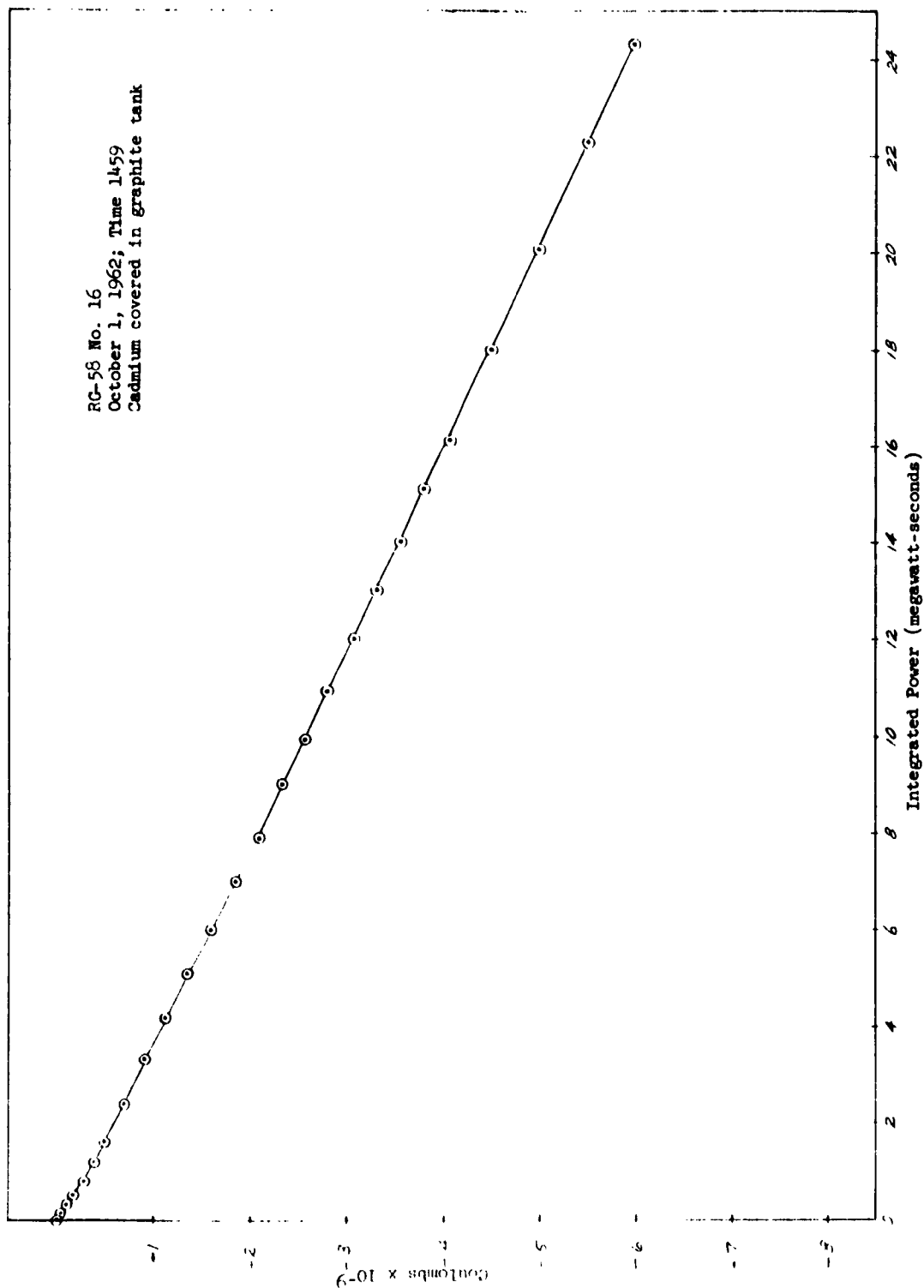


Fig. 12--Integrated signal from cadmium-covered RG-58 in graphite

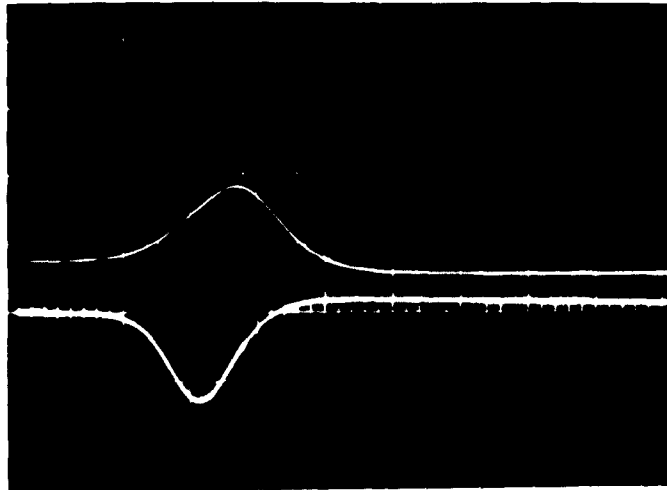
This assumes that the RG-58 cable is doubled in an experimental location about 3 ft. high, and that the vertical gamma contour is the same as in the cadmium-covered graphite. The flux value is taken at the vertical center of the cable.

#### 4.2 THERMAL NEUTRON DATA

The graphite column used to determine a value of gamma signal when the cable is wrapped in cadmium sheet is used without the cadmium to provide a radiation environment with a maximum thermal neutron flux. The gamma flux is down to about one-tenth that present in the cadmium-covered configurations. A cadmium ratio of 223 indicates a low epithermal neutron flux. Assume for the moment that any signal from fast neutrons is insignificant, and that the gamma background may be subtracted from a total signal. Figure 13 (Tr. 3678, 3679 and 3687) shows the first, second and fifth shot on an RG-cable. Note the usual time delay in the cable signal, which is compatible with the  $\text{BF}_3$  chamber measurement (See Fig. 7, Tr. 3585).

Sweep (all) - 10 msec/cm

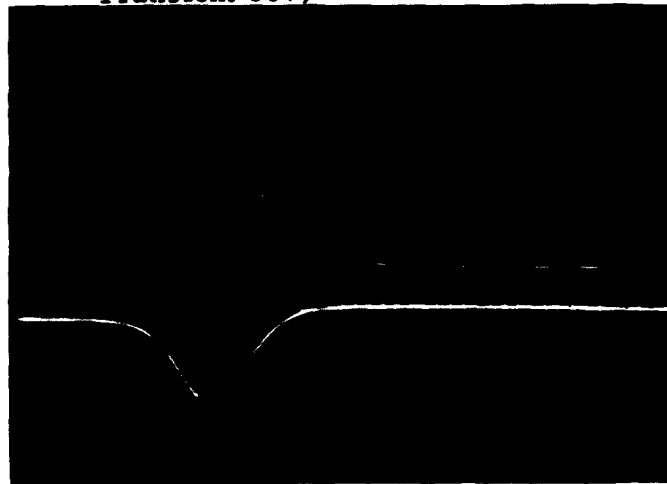
Transient 3678



RG-58 cable (1st pulse)  
10 mv/cm; +0.011 v

Reactor power  
2 v/cm; -2.5 v

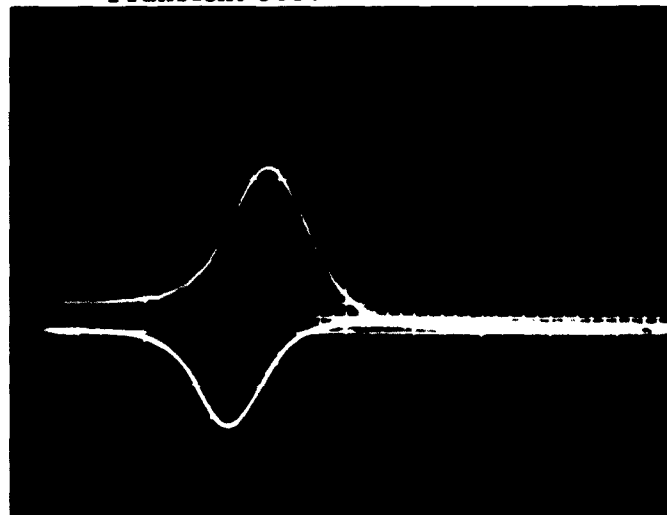
Transient 3679



RG-58 cable (2nd pulse)  
10 mv/cm; +0.010 v

Reactor power  
2 v/cm; -2.5 v

Transient 3687



RG-58 cable (6th pulse)  
5 mv/cm; +0.10 v

Reactor power  
2 v/cm; +2.8 v

Fig. 13 -- Signals from bare RG-58 in graphite tank

A steady-state run at one Mw with a bare RG-58 cable in the thermal column produced a signal shown in Fig. 14. Since the gamma present contributed a known part of the signal, this was subtracted from the resultant trace, leaving a nearly proportional signal due to neutron flux of approximately  $10^{-10}$  coulombs/Mw-sec. The slightly greater initial slope is evident. This small saturable component is opposite in sign to that seen with gamma radiation. Both are second-order effects but should be investigated in more detail.

The signal due to thermal neutron flux seems dependent on dielectric size and material. Taking a typical peak voltage of around 10 mv for RG-58 cable, the peak voltage for RG-59 cable is about 7 mv and that for Teflon RG-142 is about 30 mv, with indications of a larger initial voltage than found in polyethylene cable types.

In summary, thermal neutron fluxes produce positive signals approximately proportional to flux and dependent on size and type of dielectric.

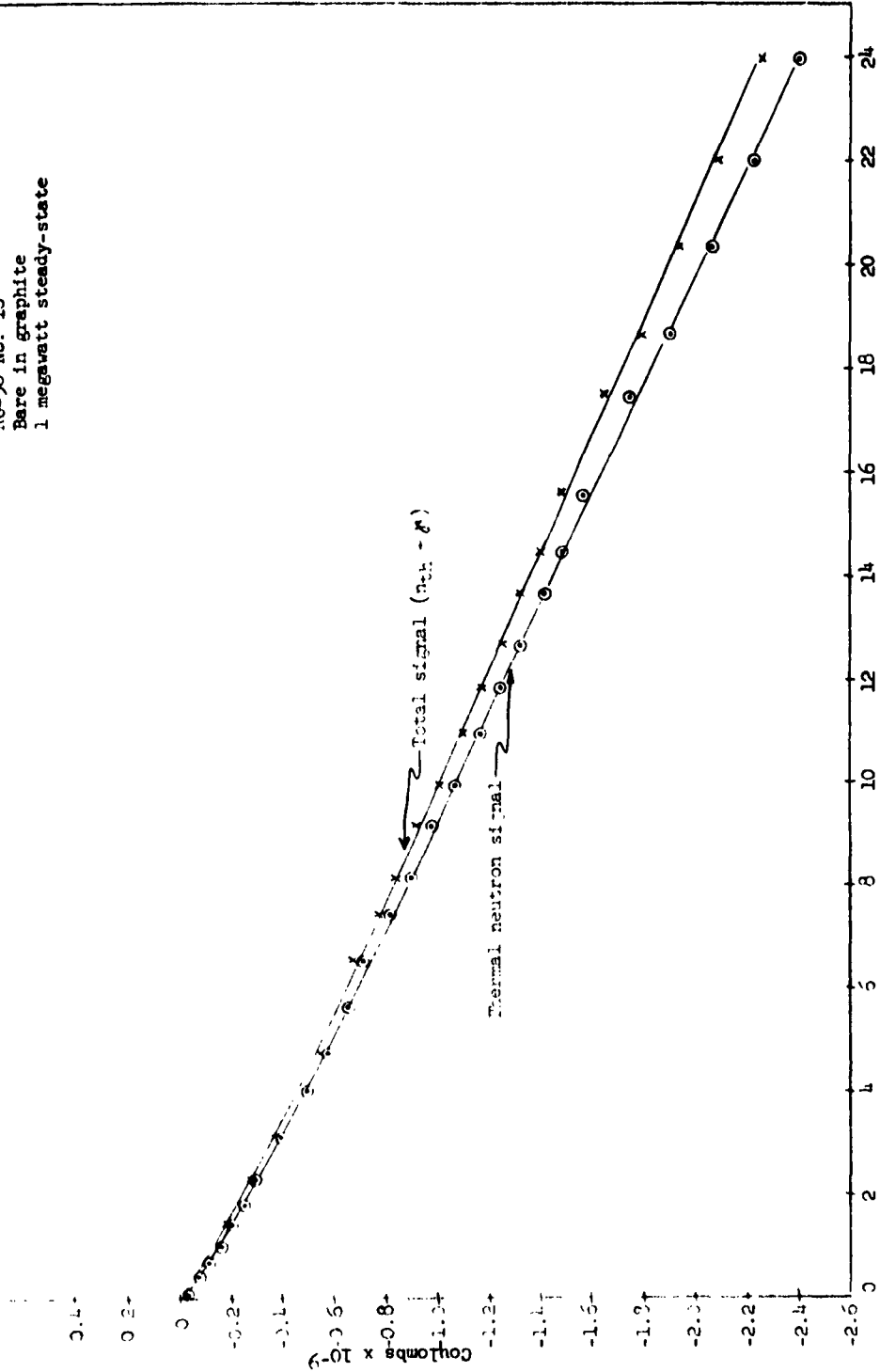
#### 4.3 FAST NEUTRON DATA

Figure 15 (Tr. 3615, 3665 and 3666) represent three typical signals from cable in the void tank. Note that the first flash produced a much larger signal, preceding the flux peak. Figure 16 summarizes the total signals taken in several pulses on an RG-58 cable. The first flash is large and indicates a very strong signal per Mw-sec on the first part of the flash. Later shots produced signals which successively decreased in height, finally going negative. The signal peaks later correspond more closely to the timing of the pulse peaks.

Figure 17 is a graph of integrated signal versus integrated power of Tr. 3615 (See Fig. 15A). Note the large change in slope during the first 20 Mw-sec which is equivalent to a single pulse. Obviously, an integrated signal would turn negative soon after the first pulse.

Using the integrator and operating the reactor at one megawatt steady-state produced a total signal shown in Fig. 18. The shape of this curve is similar to that produced in transient operation on virgin cable, with the negative slope after saturation. If  $2 \times 10^{-10}$  coulombs/Mw-sec is taken to be the gamma component of the signal, the large remaining positive-going signal is produced by the neutron flux. The residual thermal flux (<0.45 ev) produces a signal which is linear and roughly 10 percent of the fast signal.

October 1, 1962; Time 1146  
 RG-58 No. 16  
 Bare in graphite  
 1 megawatt steady-state



Integrated Power in Megawatt Seconds

Fig. 14--Integrated signal from bare RG-58 in graphite

Sweep (all) - 10 msec/cm

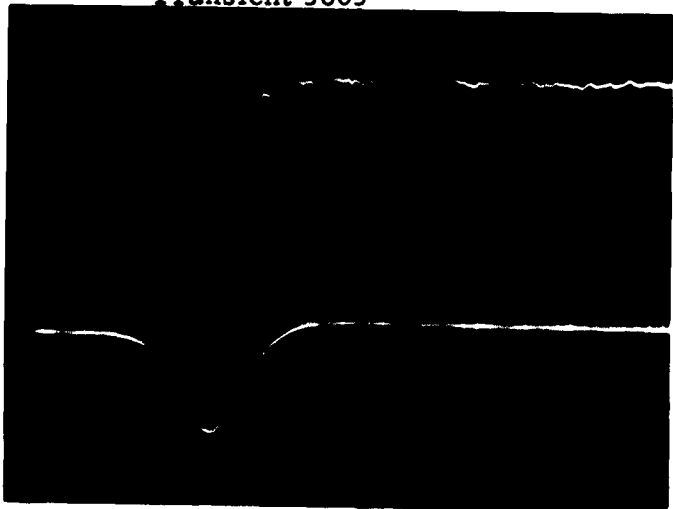
Transient 3615



RG-58 cable (1st pulse)  
10 mv/cm; +0.0135 v

Reactor power  
2 v/cm

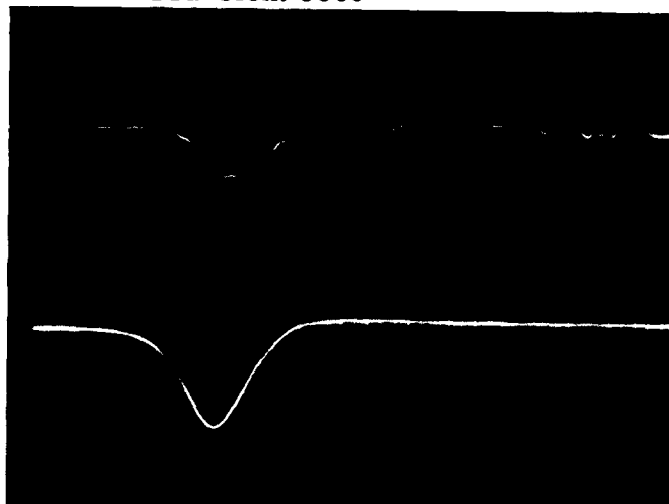
Transient 3665



RG-58 cable (6th pulse)  
1 mv/cm; +0.0004,  
-0.00035

Reactor power  
2 v/cm; -3 v

Transient 3666



RG-58 cable (7th pulse)  
1 mv/cm; -0.00075

Reactor power  
2 v/cm; 3.2 v

Fig. 15 -- Signals from bare RG-58 in void tank

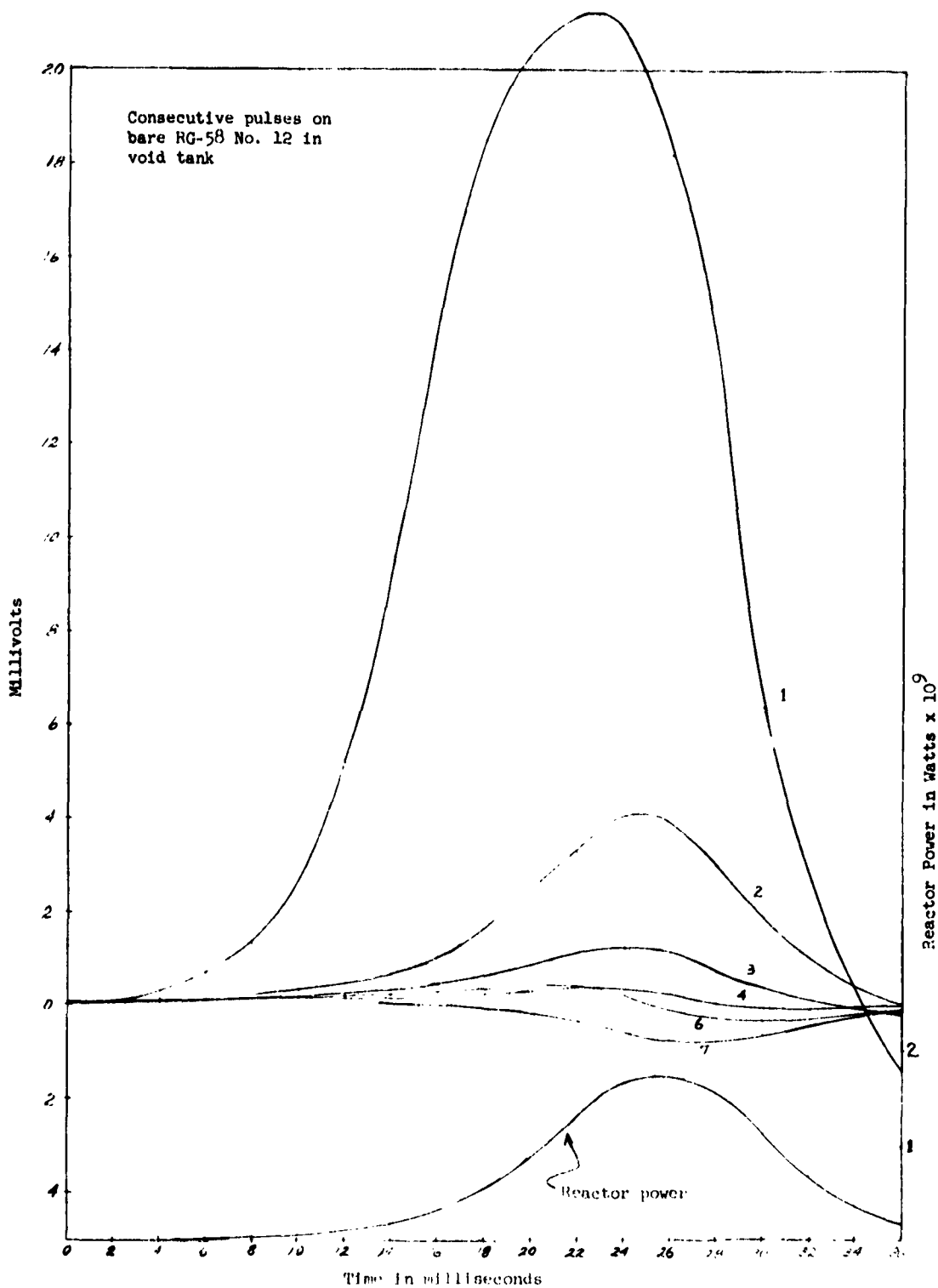


Fig. 16--Sequence of signals from bare RG-58 in void tank

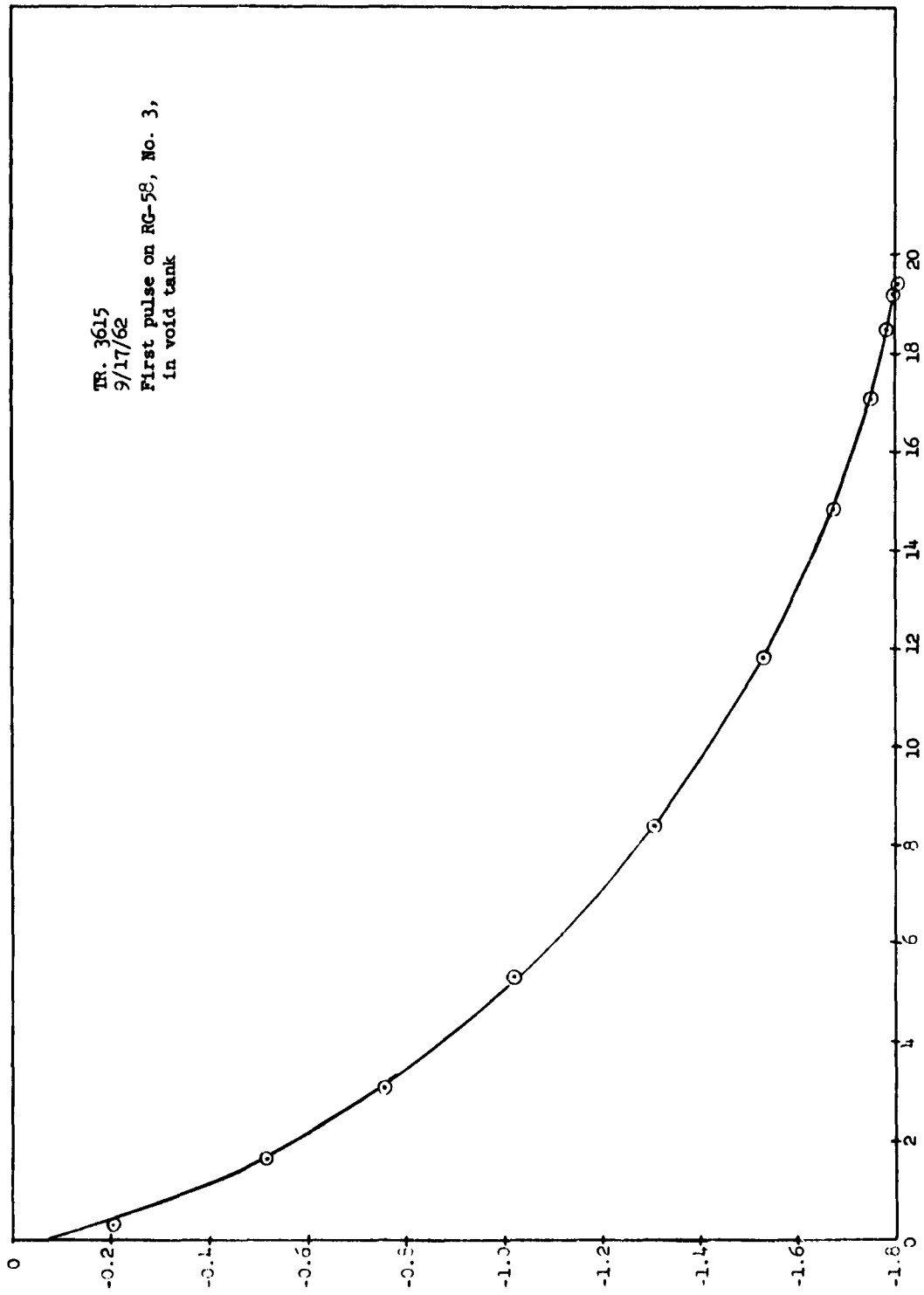


Fig. 17--Integration of signal in Fig. 15A

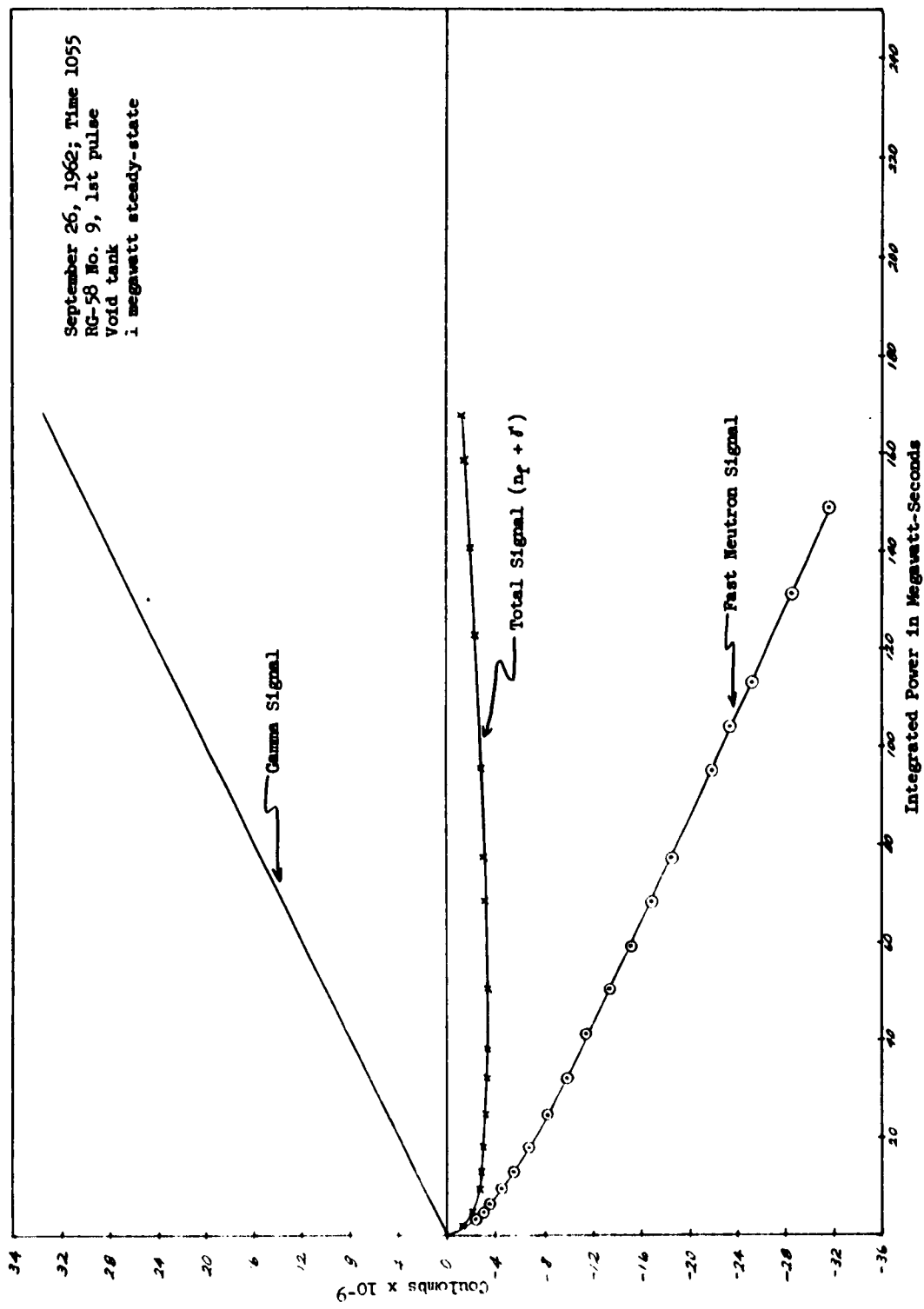


Fig. 18--Integrated signal from bare RG-58 in void tank

The remaining fast neutron signal is obviously an important radiation effect. The initial signal on virgin cable is a very large one and has a slope on the order of 20 times that on a cable saturated with fast neutrons.

Fast neutron flux produced a saturated value of signal in this run of approximately  $1.8 \times 10^{-10}$  coulombs/Mw-sec. The graph includes the signal from the thermal flux present, which amounts to less than  $10^{-11}$  coulombs/Mw-sec and may be ignored at present.

An attempt to remove the saturation of a cable by alternate charging and discharging with 300 volts was not successful. Storage of the cable overnight resulted in only a partial recovery. Other experiments are planned to investigate recovery from the saturable effect.

Several transient tests were made with voltages applied to the cables as a rough check on conductivity. The general effects appear to be complex with signal reversals but no details are included in this report. The cables exhibited conductivity in the void tank and in the graphite thermal column, and residual effects from previous flashes at different voltages were observed as found during the linear accelerator tests. Again, it is planned to make steady-state observations of conductivity in neutron flux. Perhaps some unusual conductivity effects will be noted which will aid in determining a mechanism for neutron effects.

#### 4.4 ANALYSIS OF DATA

A detailed analysis of the data in terms of possible physical mechanisms has not been made; however, a preliminary evaluation of mechanisms considered and the results are presented in this section. Experiments specifically designed to test the various possible mechanisms will no doubt be required before a final judgment can be made. The discussion is necessarily limited to signals produced with no voltage applied to the cables. Thus, both the production and net motion of charges must be included in any explanation of the effects.

##### 4.4.1 Gamma Ray Effects

Measurements of gamma-induced signals have been made previously with linear accelerators and other gamma sources, and the data are in general quantitative agreement with the results obtained here. The normalized gamma response can be calculated from the flux data. The gamma response is given as  $5.1 \times 10^{-12}$  coulombs/rad. This is for a 180-cm length of cable in the irradiation facility. The gamma dose used

was the peak for the center of the facility. If the average to peak gamma flux is taken as 0.7, the normalized reactor gamma response is calculated to be  $4 \times 10^{-14}$  coulombs/rad-cm.

The response of similar cable has been measured with 30 Mev electrons from the General Atomic LINAC. The result obtained there for the accelerator gamma response was  $2.4 \times 10^{-14}$  coulombs/rad-cm.

These two results may be considered in essential agreement because of difficulties in dosimetry over the cable lengths irradiated, and the measurement of the actual lengths of cable in the two fields. In addition, some dependence of dose rate has been seen in the response with LINAC; this may also account for some of the difference.

The gamma signal has been attributed to the ejection of Compton electrons from the shields and insulator.

The following arguments are suggested for deducing the expected size and magnitude of the gamma signal:

The production of secondary electrons by the Compton process is approximately proportional to the total number of electrons in the absorbing material. The escape of these electrons from the surface of a conducting or insulating section is determined by the energy loss of the electrons in the material. If the object considered is large compared to the range of most of the secondary electrons, it can be assumed that the number of electrons escaping from the surface is approximately proportional to the product of the rate of production and the range, since the range represents the thickness of the material near the surface which is contributing electrons that may escape. The range is, to the first order, inversely proportional to the electron density in the material. The first correction term to this relation is a logarithmic dependence upon  $Z$ , the charge per atom, which tends to make the range somewhat larger in high  $Z$  materials than the first-approximation value.

In the first approximation, the  $Z$  dependence of the Compton production and the inverse  $Z$  dependence of the range cancel out, predicting a secondary emission which is independent of the nature of the absorbing material. The correction term in the energy loss formula tends to make the secondary emission somewhat larger for higher  $Z$  materials. Furthermore, if the object is not thicker than the range of the maximum-energy Compton electron, the secondary emission from high  $Z$  materials again tends to be larger than the emission from lower  $Z$  materials. Hence, in the comparison between the secondary emission

from the polyethylene dielectric in a coaxial cable and the copper center conductor and shield, it is expected that the secondary emission from the copper will be somewhat larger than the emission from the polyethylene. A net current of electrons is therefore expected to go into the insulator. The signal induced in the center wire with the shield grounded is expected to have two components; the first is a positive component due to a net emission of electrons from the center wire into the insulator, and the second is a negative component due to a net emission of electrons into the insulator from the shield. If one assumes again that the range of these secondary electrons is very small compared to either the diameter of the center wire or shield, one finds that the two terms cancel out if the emission per unit area from the center wire is the same as the emission per unit area from the shield. The reason for this cancellation is that the motion of a charge a given distance near the center wire induces a charge in the center conductor which is larger by the ratio of the radii than that charge induced by a motion of equivalent distance near the shield. On the other hand, the total number of electrons performing this motion is larger near the shield by the same ratio as the ratio of shield to center wire radii. On the other hand, if one assumes that the radius of the center wire is not very large compared to the range of the electrons but that the radius of the shield is large compared to the range of the electrons, then the next correction term makes the signal induced in the center wire (due to the electrons emitted from it) somewhat less than the signal due to the electrons emitted from the shield. A net negative signal is therefore predicted. The magnitude of this signal depends on the absolute difference in secondary emission coefficients of the polyethylene and copper as well as the distances the electrons travel in the insulator. Since total emission coefficients of the order of 0.5 to 1 percent of the incident photon flux are reasonable, it might not be surprising to observe a signal in which the effective charge removed from the central wire is of the order of 0.1 percent of the photons intercepted by the coaxial cable. This estimate is not inconsistent with the experimental results, but obviously must be checked more accurately before the mechanism can be established conclusively.

#### 4.4.2 Thermal Neutron Effects

The thermal neutron response of  $10^{-10}$  coulombs/Mw-sec can be converted to other units so that a comparison can be made with the thermal neutron events taking place in the cable. For this analysis, consider only the peak rate occurring during the pulse (peak reactor power equals 1600 Mw). This signal therefore represents a charge transfer rate of  $10^{12}$  electronic charges/sec. Further, the peak power generated by the cable would be  $2.6 \times 10^{-9}$  watts.

These rates apply for a measured thermal neutron flux of approximately  $10^{14}$  nv in the center of the exposure region (See Table 1). It is of interest to calculate the rates of the various thermal neutron interactions in the cable. The following three separate processes will be calculated:

- (1) Capture by the hydrogen in the polyethylene,
- (2) Capture by the copper in the central wire and shield,
- (3) Scattering by the hydrogen in the polyethylene.

For these purposes, consider the irradiation to be for 6 ft. of cable, and the axial average flux in the graphite facility to be 0.7 times the peak flux. Thus, the average flux is  $6.6 \times 10^{13}$  nv. The volume of polyethylene in cable is 11.5 cm<sup>3</sup>, and the volume of copper is 0.95 cm<sup>3</sup>. Polyethylene contains  $6.9 \times 10^{22}$  H atoms/cm<sup>3</sup> giving  $7.9 \times 10^{23}$  H atoms in the irradiated cable. The cross section for hydrogen capture is 0.33 barns. Thus the number of H capture events per second for the average flux of  $6.6 \times 10^{13}$  nv is  $1.7 \times 10^{13}$ . The rate of capture in copper central wire can be similarly calculated to be  $2.0 \times 10^{13}$ , and the shield capture rate is  $5.7 \times 10^{13}$ .

It is also of interest to calculate the number of thermal neutron scattering events for neutrons of energy  $> 0.14$  ev and  $< 1$  ev. Data for this calculation have been obtained from computation of the neutron spectrum in graphite. The result is:

$$\text{H scattering events between } 0.14 - 1 \text{ ev/sec} = 6.96 \times 10^{13}.$$

The physical processes by which these nuclear interactions could produce an electrical effect are open to postulation, and some possible mechanisms will now be considered. Neutron capture by hydrogen results in the emission of a 2.2 Mev gamma ray and the formation of a deuteron. The gamma ray is not expected to have any unusual effect, and in fact should contribute to a negative signal rather than the positive signal observed. The relatively high gamma energy and the small density of electrons eliminate any significant contribution from internal conversion electrons. The deuteron, however, will have a recoil energy of 1.3 kev. The deuteron would produce electron ionization with a maximum electron energy of 1.3 ev minus the binding energy of the electron. This is a very small energy and probably would not produce any significant number of electrons since the electron binding energy is expected to be  $\sim 10$  eV, which is considerably greater than the energy available. Proton recoils of maximum energy of 1.16 kev

would also be produced. Both the protons and the original deuterons could produce a net charge transfer; however, the range of each is quite short. The central wire would act as a sink for positive charges since none would be emitted from copper. The charge efficiency required is 5.8 percent. That is, 5.8 percent of the hydrogen captures result in the net transfer of one electronic charge across the cable. This is quite high considering the ranges and energies involved.

Thermal neutron capture in copper produces capture gammas over a wide range of energies. About 50 percent of the captures result in a gamma of less than 1 Mev in energy. These in turn could produce an internal conversion electron, emitted from the copper. The charge efficiency for this process would need to be about 5 percent considering only captures in the central wire. This is quite high for an internal conversion efficiency with the high energy gamma rays. The internal conversion efficiency for a 1 Mev gamma is very small ( $\sim 10^{-3}$  percent) for an atom with this mass. A detailed analysis of the gamma spectrum of copper may show this effect to be more probable than indicated in this preliminary treatment.

The scattering of thermal neutrons from hydrogen may produce a large number of protons of energy less than 0.45 ev, the cadmium cut off energy. These low energy protons could produce a charge transfer. Work done by Mayburg and Lawrence <sup>(1)</sup> on the temperature dependence of the conductivity of polyethylene in a gamma field (cobalt source) has led to an interpretation of ionic conduction by protons. They compute the "activation" energy required to produce a free proton charge to be 0.13 ev. Thus on the basis of this model, the higher-energy subcadmium neutrons would produce free protons. The efficiency of charge collection would then be 1.4 percent for neutrons between the energies of 0.14 to 1 ev. This range is used because computations of the spectrum were available. This possible mechanism cannot, therefore, be eliminated on an efficiency basis alone. The explanation given by Mayburg and Lawrence for the conductivity in polyethylene is not unique in the light of more recent understanding of the conductivity in insulators. The effects they observed can be explained with electronic rather than ionic conduction. The transfer of charge by such a low energy proton is difficult to understand; however, more experimental information should provide an answer.

The overall sensitivity to thermal neutrons can be calculated as  $1.3 \times 10^{-23}$  coulombs/nvt-cm. At this time the mechanism for producing an electrical signal with thermal neutron irradiation is not clear. Further experiments will be performed to obtain more information on the possible mechanism.

#### 4.4.3 Fast Neutron Effects

Two phenomena are apparent from the fast neutron irradiation; the first is an effect which saturates with fast neutron dose, and the second is an effect which is independent of total dose. Both effects give a positive signal. A graphical separation of the two effects was done to provide a measure of the relative sensitivities, thus determining the initial and final slopes of the curves. These are  $3.6 \times 10^{-9}$  coulombs/Mw-sec and  $1.8 \times 10^{-10}$  coulombs/Mw-sec respectively. In addition, the saturable component was fitted by the method of least squares to the form  $y = a(1 - bd^{-cx})$ . The fit was of the right shape, although somewhat poor in detail as can be seen from Fig. 19. This may have been due to inaccuracies in the data and further attempts will be made.

In this fit, the following numerical values for the constants were:

$$a = 4.7 \times 10^{-9} \text{ coulombs}$$

$$b = 0.85$$

$$c = 0.076 (\text{Mw-sec})^{-1}$$

Note that the constant b is close to unity; however, with b not unity, the initial slope of the fitted curve is not valid. The constant can be normalized from data presented later in this section. Particularly, the saturated charge, a, is better expressed per unit length and is:

$$a = 2.6 \times 10^{-11} \text{ coulombs/cm.}$$

This, of course, is independent of dose and possibly dose rate, since the recovery time was found to be very long. The charging constant c can be converted to other more useful units also. The results for flux greater than 10 kev are:

$$c = 1.9 \times 10^{-4} \text{ rad}^{-1}$$

and  $c = 3.0 \times 10^{-13} (\text{nvt})^{-1}$ .

September 26, 1962; Time 1055  
RG-58 No. 9  
Void tank  
1 megawatt steady-state

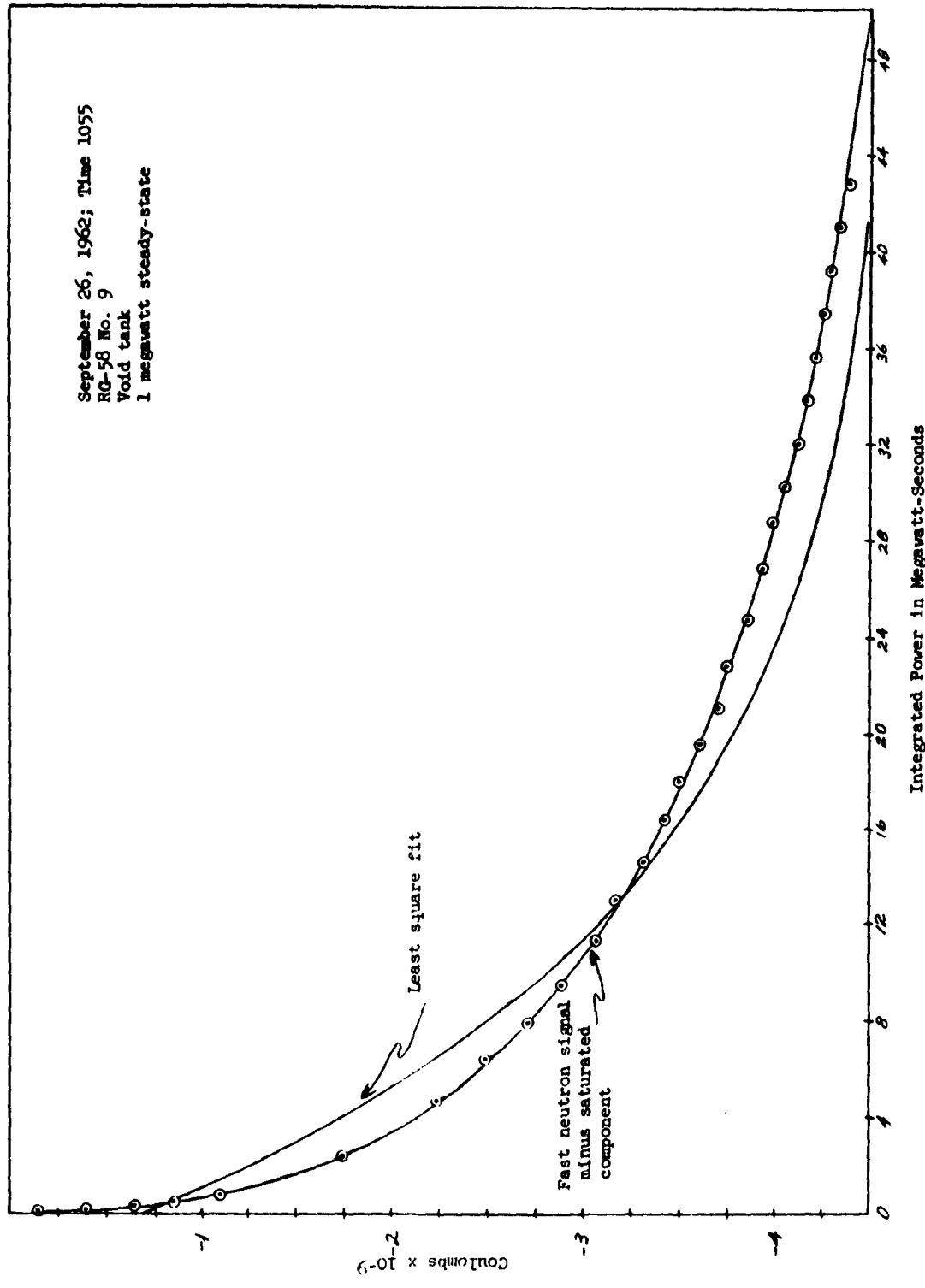


Fig. 19--Prompt component of fast neutron signal in RG-58

It is not known whether the fast neutron response results from a single mechanism or from two or more mechanisms. It is tempting to postulate two mechanisms for the saturable and linear responses. The linear response could be due to fast neutron capture in hydrogen and/or copper. This would be the same process as discussed in Section 4.4.2. A reasonable speculation would be that the exponential portion is due to scattering by the protons; this is also similar to that discussed in Section 4.4.2 except that proton energies up to a few Mev would be produced. The fact that fast neutron irradiation does not change the sensitivity of the cable to either thermal neutrons or gamma rays is at least indicative of a different mechanism for the saturable effect.

Estimates of the total fast neutron flux in the exposure facility were obtained by preliminary foil saturation measurements of fission foils and sulfur. The calculated neutron spectrum within the core was used to extend the values from the lowest threshold of 10 kev down to 1 ev. The average flux over the vertical 36 in. irradiation zone has been previously measured to be 0.8 times the peak flux. The following values represent the average flux and are given per Mw-sec:

$$\phi (> 2.5 \text{ Mev}) = 1.2 \times 10^{10} \quad (\text{Measured})$$

$$\phi (> 10 \text{ kev}) = 2.5 \times 10^{11} \quad (\text{Measured})$$

$$\phi (> 1 \text{ ev}) = 4.0 \times 10^{11} \quad (\text{Calculated})$$

Note that the value for the sulfur flux (given in Table 1) is for a 20 Mw-sec pulse. One-group cross sections for the energy range 1 ev to 10 Mev have been obtained, for hydrogen capture and scattering and for copper capture, for the same spectrum so that the number of these events may be calculated. The results for 183 cm of cable are:

$$\text{Hydrogen captures} = 7.8 \times 10^8 / \text{Mw-sec}$$

$$\text{Hydrogen scattering} = 3.4 \times 10^{12} / \text{Mw-sec}$$

$$\text{Copper capture (central wire)} = 3.3 \times 10^9 / \text{Mw-sec}$$

$$\text{Copper capture (shield)} = 9.1 \times 10^9 / \text{Mw-sec}$$

The total dose from fast neutrons can also be calculated from the foil measurements to be 400 rads/Mw-sec. The estimate of the uncertainty of this figure is less than a factor of 2.

The initial and saturated fast neutron sensitivities of  $3.6 \times 10^{-9}$  and  $1.8 \times 10^{-10}$  coulombs/Mw-sec may now be normalized to the events occurring in the cable and the efficiencies calculated, as was done with the thermal neutron effect (refer to Section 4.3.2). The response per rad-cm is of interest for comparison with the gamma effect and data obtained with other facilities. The result is:

$$\text{Fast neutron response (initial)} = 4.9 \times 10^{-14} \text{ coulombs/rad-cm}$$

$$\text{Fast neutron response (saturated)} = 2.5 \times 10^{-15} \text{ coulombs/rad-cm.}$$

These can now be compared with the gamma response of  $4 \times 10^{-14}$  coulombs/rad-cm. The initial neutron value is approximately equal to the gamma sensitivity and the saturated value lower by a factor of 20.

The responses can also be compared on a charge basis with the nuclear events in the cable. The charge transfer rates are:

$$\text{Initial} = 2.25 \times 10^{10} \text{ electronic charges/Mw-sec}$$

$$\text{Saturated} = 1.1 \times 10^9 \text{ electronic charges/Mw-sec.}$$

These can now be compared with the interaction rates calculated above. The ratios of charge transfer to the nuclear events for the various processes is given in Table 2. The figures in the table represent the number of charges that must be collected per nuclear event. If the number is greater than unity, then secondary processes must occur and provide charge multiplication if the mechanism is to be a valid one. If only primary processes are considered, it appears that hydrogen scattering with proton production is the only mechanism of these, which could account for the initial fast neutron effect. The capture events can be compared in efficiency with those calculated for the thermal neutron response. Since thermal neutron capture represents a high energy effect from the reaction energy, the response should be relatively insensitive to neutron energy. Thus, the efficiencies of ~ 5 percent required for the thermal neutron effect are to be compared with efficiencies of 250 to 3200 percent for the initial fast neutron effect. From these arguments, the conclusion is drawn that hydrogen scattering is the most likely mechanism for the initial fast neutron effect.

Table 2  
FAST NEUTRON EFFECTS

	<u>Charge Transfer Rate</u> <u>Nuclear Event Rate</u>	
	<u>Initial Response</u>	<u>Saturated Response</u>
Hydrogen Scattering	0.0066	0.0003
Hydrogen capture	32	1.4
Copper capture (central wire)	6.8	0.33
Copper capture (shield)	2.5	0.12

Similar arguments and comparisons can be made for the saturated fast neutron effect. In this case, it appears that any of the mechanisms could be responsible for the response. A more detailed analysis of possible copper capture mechanisms should be made. Particularly, the copper captures in the shield and central wire should be competing effects so that the difference in rate would be a better comparison. The result is about 65 percent of the shield capture rate. Experiments are in progress to give more information on a possible mechanism.

## V CONCLUSIONS

The following cable effects have been observed and identified:

1. Gamma radiation produces a current proportional to flux, the central wire going negative with respect to the shield. In RG-58 cable, the gamma response was found to be about  $4 \times 10^{-14}$  coulombs/rad-cm in the TRIGA reactor, and  $2.4 \times 10^{-14}$  coulombs/rad-cm in the General Atomic Linear Accelerator. The gamma sensitivity was found to remain essentially independent of previous exposure to gamma rays or neutrons.
2. The thermal neutron effect in the cable produces a response proportional to dose, with the opposite polarity to gamma response. The signal is also independent of previous irradiation with either neutrons or gammas. The sensitivity was measured as  $1.3 \times 10^{-23}$  coulombs/nvt-cm.
3. Fast neutron irradiation also produces a response in cable of opposite polarity to gamma effect. A large initial response was found which rapidly saturated. A residual response remained and was approximately linear with dose. The initial sensitivity found was  $4.9 \times 10^{-14}$  coulombs/rad-cm, and the saturated response was  $2.5 \times 10^{-15}$  coulombs/rad-cm in RG-58 cable, a difference of about a factor of 20. Measurements showed the recovery time for the saturable effect to be greater than one day.
4. The effects outlined above were not found to be rate-sensitive; that is, signals per MW-sec were comparable during both pulsing and steady-state operation of the TRIGA reactor.

Preliminary measurements with voltage applied to the cable show such characteristics as signal reversals during the pulse and memory effects from previous irradiation. Further measurements will be made to classify these effects. In addition, experiments are planned to investigate the several possible mechanisms for the effects.

## VI ACKNOWLEDGEMENTS

The contributions of several persons are gratefully acknowledged. V. A. J. van Lint provided much valuable guidance and contributed to many discussions during the course of this work. J. Shoptaugh and C. Coffey operated the reactor and provided dosimetry information. The support of the Signal Corps, U. S. Army, and particularly E. Both, C. P. Lascaro, and Wm. Schlosser is appreciated. G. West provided the computed neutron flux and spectra data used in this report.

## REFERENCE

1. Mayburg and Laurence, J. Applied Phys. 25, 1006 (1952)

UNITED STATES ARMY SIGNAL RESEARCH &  
DEVELOPMENT LABORATORY  
DISTRIBUTION LIST  
RESEARCH AND DEVELOPMENT CONTRACT REPORTS

	<u>Number of copies</u>
Technical Library OASD (R&E) Rm 3E1065 The Pentagon Washington 25, D. C.	1
Chief of Research and Development OCS, Department of the Army Washington 25, D. C.	1
Chief Signal Officer Department of the Army Washington 25, D. C. Attn: SIGRD	1
Director, U.S. Naval Research Laboratory Washington 25, D. C. Attn: Code 2027	1
Commanding Officer and Director U. S. Navy Electronics Laboratory San Diego 52, California	1
Commander, Aeronautical Systems Division Wright-Patterson Air Force Base Ohio Attn: ASAPRL	1
Commander, Air Force Cambridge Research Laboratories, L. G. Hanscom Field Bedford, Massachusetts Attn: CRO	1
Commander, Air Force Command and Control Development Division, L. G. Hanscom Field, Bedford, Massachusetts Attn: CRZC	1

	<u>Number of copies</u>
Air Force Command and Control Development Division, L. G. Hanscom Field, Bedford, Massachusetts Attn: CCRR & CCSD	2
Commander, Rome Air Development Center Griffiss Air Force Base New York Attn: RAALD	1
Commander, Armed Services Technical Information Agency Arlington Hall Station Arlington 12, Virginia Attn: TIPCR	10
Chief, U. S. Army Security Agency Arlington Hall Station Arlington 12, Virginia	2
Deputy President U. S. Army Security Agency Board Arlington Hall Station Arlington 12, Virginia	1
Commanding Officer Diamond Ordnance Fuze Laboratories Washington 25, D. C. Attn: Library, Rm. 211, Bldg. 92	1
Commanding Officer U. S. Army Signal Equipment Support Agency Fort Monmouth, N. J. Attn: SIGMS-ADJ	1
Corps of Engineers Liaison Office U. S. Army Signal Research and Development Laboratory Fort Monmouth, N. J.	1

	<u>Number of copies</u>
AFSC Liaison Office Naval Air R&D Activities Command Johnsville, Pennsylvania	1
Marine Corps Liaison Office U. S. Army Signal Research & Development Laboratory Fort Monmouth, N. J. Attn: SIGRA/SL-LNR	1
Commanding Officer U. S. Army Signal Research & Development Laboratory Fort Monmouth, N. J. Attn: Director of Research	1
Commanding Officer U. S. Army Signal Research & Development Laboratory Fort Monmouth, N. J. Attn: Technical Documents Center	1
Commanding Officer U. S. Army Signal Research & Development Laboratory Fort Monmouth, N. J. Attn: SIGRA/SL-ADJ (MF&R Unit No. 1)	1
Advisory Group on Electron Devices 346 Broadway New York 13, New York	2
Commanding Officer U. S. Army Electronic Research & Development Laboratory Fort Monmouth, N. J. Attn: SELRA/SL-TNR (FOR RETRANSMITTAL TO ACCREDITED BRITISH AND CANADIAN GOVERNMENT REPRESENTATIVES)	3

	<u>Number of copies</u>
International Business Machines Corporation Federal Systems Division Attn: Mr. Wm. Bohan Owego, New York	1
Hughes Aircraft Company Fullerton, California Attn: Mr. J. D. Faith	1
Commanding Officer, U. S. Army Electronic Research & Development Laboratory Fort Monmouth, N. J. Attn: SELRA/SL-PEE (Mr. Wm. Schlosser)	1
Capt. Donald C. Glenn Air Force Special Weapons Center Kirtland Air Force Base Albuquerque, New Mexico	1
Commanding Officer, Diamond Fuze Laboratories Connecticut Avenue and Van Ness Street, N. W. ATTN: Chief, Nuclear Vulnerability Branch (230) Washington 25, D. C.	1
Commanding Officer U. S. Army Signal Research and Development Laboratory ATTN: SIGRA/SL-P, Fort Monmouth, New Jersey	1
Commanding Officer Naval Ordnance Laboratory ATTN: Dr. Bryant Corona, California	1
Commander Naval Ordnance Laboratory, White Oak ATTN: Mr. Grantham Silver Spring, Maryland	1

	<u>Number of copies</u>
Commander U. S. Naval Material Laboratory New York Naval Shipyard Naval Base, Brooklyn 1, New York	1
Commanding Officer and Director U. S. Naval Radiological Defense Laboratory San Francisco 24, California	1
AFSWC (SWRPA) Kirtland AFB, New Mexico	1
AFSWC (SWRPL) Kirtland AFB, New Mexico	1
Chief Defense Atomic Support Agency ATTN: DASARA-4 Washington 25, D.C.	1
President Sandia Corporation Sandia Base Albuquerque, New Mexico ATTN: Dr. C. D. Broyles, 5113	1
President Sandia Corporation Sandia Base Albuquerque, New Mexico ATTN: Dr. J. W. Easley, 5300	1
President Sandia Corporation Sandia Base Albuquerque, New Mexico ATTN: S. C. Rogers, 5312	1
Director Advanced Research Projects Agency Washington 25, D. C. ATTN: LtCol. Roy Woidler	1

Number  
of copies

Admiral Corporation  
3800 Cortland Street  
Chicago 47, Illinois  
ATTN: Mr. R. Whitner 1

Applied Physics Laboratory  
Johns Hopkins University  
8621 Georgia Avenue  
Silver Spring, Maryland  
ATTN: Mr. Robert Frieberg  
Via: BuWeps Representative, APL/JHU  
Silver Spring, Maryland 1

North American Aviation Corporation  
Atomics International Division  
21600 Van Owen Street  
Canoga Park, California  
ATTN: Dr. A. Saur 1

ARINC Research Corporation  
1700 K Street, N. W.  
Washington 6, D. C.  
ATTN: Mr. W. Schultz 1

Burroughs Corporation  
Central Avenue and Route 202  
Paoli, Pennsylvania 1

General Dynamics/Fort Worth  
Convair Division  
Grants Land  
Fort Worth 1, Texas  
ATTN: Mr. E. L. Burkhard 1

General Electric Company  
Receiving Tube Department  
1301 East 18th Street  
Owensboro, Kentucky  
ATTN: Mr. D. Mickey 1

	<u>Number of copies</u>
General Electric Microwave Department 130 Saratoga Road Schenectady, New York ATTN: Mr. A. Hodges	1
Georgia Institute of Technology and Engineering Experiment Station 722 Cherry Street, N. W. Atlanta 13, Georgia ATTN: Dr. R. B. Belser	1
Hughes Aircraft Company Florence and Teale Streets Culver City, California ATTN: Mr. T. D. Hanscome	1
Hughes Aircraft Company Florence and Teale Streets Culver City, California ATTN: Dr. C. Perkins	1
International Business Machine Corporation Federal Systems Division Route 17C Owego, New York ATTN: Mr. Bohan	1
Radiation Effects Information Center Battelle Memorial Institute 505 King Avenue Columbus 1, Ohio ATTN: Mr. E. N. Wyler	1
Northrop Corporation Ventura Division 8000 Woodley Ave. Van Nuys, California ATTN: Dr. D. A. Hicks	1

	<u>Number of copies</u>
Space Technology Laboratories P. O. Box 95001 Los Angeles 45, California ATTN: Dr. B. Sushols, Mr. J. Maxcy Thru: DCAS, AF Unit Post Office ATTN: TDC 61-1019-4 Los Angeles, California	2
Sperry Microwave Electronics Company San Christopher Drive (H. P. Hood and Sons, Inc.) Plant Dunedin, Florida ATTN: Dr. Gordon Harris	1
Stevens Institute of Technology 501 and 711 Hudson Street Hoboken, New Jersey ATTN: Dr. E. Hanley	1
The Boeing Company, Aerospace Division Physics Technology Dept. 7755 E. Marginal Way Seattle 8, Washington ATTN: Dr. Glenn Keistor	
D. M. Newell, Dept. 52-10, 204 Lockheed Missiles and Space Company 3251 Hanover Street Palo Alto, California	1
Mr. B. Susholz Space Technology Laboratories, Inc. One Space Park Redondo Beach, California	1
President Sandia Corporation Sandia Base Albuquerque, New Mexico ATTN: A. W. Snyder, 5313	1